J. Fluid Mech. (1997), *vol.* 341, *pp.* 59–76. Printed in the United Kingdom

Propagation of strongly nonlinear plane N-waves

By YOSHINORI INOUE AND TAKERU YANO

Department of Engineering Science, Faculty of Engineering, Hokkaido University, Sapporo 060, Japan

(Received 21 November 1995 and in revised form 20 January 1997)

Formation and evolution of N (-like) waves is studied without the restriction of low amplitude, namely weak nonlinearity. To this end, the classical piston problem of gasdynamics is investigated, in which the wave is radiated by a piston executing a single cycle of harmonic oscillation into an inviscid perfect gas. The method of analysis is based on the simple-wave theory up to the shock formation time, and beyond that time on the numerical calculation by a high-resolution TVD upwind scheme. The initial sinusoid-like wave profile is rapidly distorted as the wave propagates, and this leads to the formation of head and tail shocks. The main effects of strong nonlinearity may be listed as follows: (i) entropy production at shock fronts, (ii) the existence of waves reflected from shocks, (iii) an asymmetric wave profile stemming from the boundary condition at the source of the strongly nonlinear problem. As the result, the strongly nonlinear wave possesses the following remarkable distinctive features, in contrast to its counterpart in the weakly nonlinear regime. The tail shock is not formed at the tail of the wave, and the expansion wave behind the head shock has non-uniform intensity. The N (-like) wave propagates with some excess mass. Thereby a region with low density, associated with the entropy production, appears in the vicinity of the source.

1. Introduction

The N-wave is one of the most typical nonlinear waves in gasdynamics as well as in nonlinear acoustics (for example, see Lighthill 1956, 1978; Whitham 1974; Rudenko & Soluyan 1977; Sachdev 1987). The problem of sonic booms generated by an aircraft moving at supersonic speed has much stimulated the progress of N-wave theory (Lighthill 1971; Hayes 1971; Pierce 1993). In that case, a simplified version of the axisymmetric N-wave applies. A large number of papers have been published on the study of the N-wave (see below), but as far as the present authors know, the studies in the literature are confined to the weakly nonlinear regime. In this paper we shall deal with the formation and evolution of strongly nonlinear plane N-waves in the case where we can neglect the dissipative effect everywhere except for discontinuities, i.e. shock fronts. To be more precise, we assume that the wave is emitted into a semi-infinite space filled with a uniform perfect gas, by the sinusoidal motion of an infinite plate (piston) during a single period.

The wave phenomenon under consideration can be precisely designated in terms

of the acoustic Mach number M and the acoustic Reynolds number Re:

$$M \equiv \frac{u_0}{c_0} = O(1) \quad \text{and} \quad Re \equiv \frac{(\gamma+1)c_0 u_0}{\delta\omega} \gg 1, \tag{1.1a,b}$$

where $u_0 = a\omega$ is the maximum speed of the source (a is the displacement amplitude of the source and ω is the angular frequency of oscillation), c_0 is the speed of sound in the initial undisturbed gas, γ is the ratio of specific heats for the perfect gas, and δ is the diffusivity of sound (see Lighthill 1956), given as $\delta = \nu[\frac{4}{3} + (\zeta/\eta) + (\gamma-1)\kappa/\eta c_p]$ ($\nu \equiv \eta/\rho_0$ is the kinematic viscosity, ρ_0 is the density in the initial undisturbed gas, η is the viscosity, ζ is the bulk viscosity, κ is the thermal conductivity, and c_p is the specific heat at constant pressure). Condition (1.1a) means that the wave concerned is a strongly nonlinear one, and condition (1.1b) means that we can regard a shock wave as a discontinuity and may ignore the dissipative effect elsewhere.

At present, the conventional weakly nonlinear theory in the limit as $M \to 0$ has been well-established for the N-wave problem. The N-wave, which appears at large distances from a body of revolution or a two-dimensional body moving with a velocity exceeding that of sound, has been studied by the following pioneers: Landau (1945), DuMond *et al.* (1946), Friedrichs (1948), and Whitham (1950). One can analyse such a problem using the method of characteristics together with the famous equal-areas rule, because the acoustic Reynolds number is ideally considered as infinity in this case. The effect of a finite acoustic Reynolds number on plane progressive waves can be elucidated by solving the Burgers equation, which was first derived by Mendousse (1953) for viscous fluids and by Lighthill (1956) for thermoviscous perfect gases. The Burgers equation is solvable by the Cole–Hopf linearizing transformation, so that various plane waves have so far been handled in this way. The propagation of cylindrical and spherical outgoing waves is governed by generalized Burgers equations. The asymptotic behaviour of spherical and cylindrical N-waves involved with the phase after long time has been investigated in detail by making use of a matched asymptotic approach (Crighton & Scott 1979) and the numerical method (Sachdev, Tikekar & Nair 1986). In the laboratory, N-shaped shock pulses were first generated in a circular pipe by a transducer of electro-magnetic induction type (Nakamura & Takeuchi 1969).

In weakly nonlinear theory for high acoustic Reynolds number, the initial one-cycle sinusoidal waveform is slowly distorted as the wave propagates and this leads to the formation of two shocks in the far field (see §3). Then it evolves into the well-known balanced N-wave whose amplitude is progressively attenuated, and whose length progressively increases.

Few studies of the strongly nonlinear problem with $M = O(1)$ have been done in the field of gasdynamics (nonlinear acoustics). In a perfect fluid, the wave motion up to the instant of shock formation is a simple wave. The problem of a simple wave produced by arbitrary motion of a piston in a long tube was first solved by Earnshaw (1860). The Earnshaw exact plane wave solution can readily be applied to a typical problem in which the source begins to execute sinusoidal motion at the time $t = 0$ and then continues (Blackstock 1962).

As pointed out by Landau (1945), the appearance of reflected waves behind the shock, together with entropy production at the shock front, render the simple-wave assumption invalid after the shock formation time (see also Courant & Friedrichs 1948). In order to handle such a complex (strongly nonlinear) problem, the present authors employ the Osher–Chakravarthy numerical scheme, a high-resolution upwind finite difference scheme widely used nowadays in the field of gasdynamics (Osher &

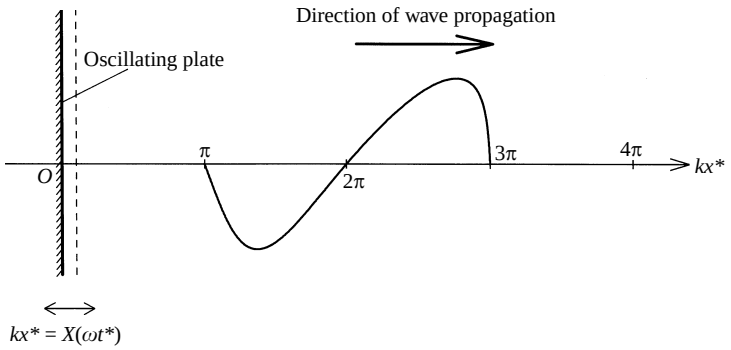

FIGURE 1. Schematic of the model: generation of the strongly nonlinear wave.

Chakravarthy 1986) and applied previously to the problem by us (Inoue & Yano 1990, 1993). It was shown that the asymptotic wave profile in the far field evolves into a sawtooth-like wave, except for the leading phase in a half-cycle. In marked contrast to the sawtooth wave in the weakly nonlinear theory, the waveform is unsymmetric between the rarefactive phase and the compressive phase. We remark that this lack of symmetry is due purely to the specification of u on the displaced piston. Also the shocks eventually coalesce. The generated shock waves induce unidirectional and almost steady streaming, which would continue to rarify the gas in the region near the source. By the same numerical method, we have dealt with the strongly nonlinear problem of a harmonically pulsating sphere (Yano & Inoue 1994) and that of a harmonically oscillating circular piston mounted in an infinite plane wall (Yano & Inoue 1993). Also, it is worth noting that the strongly nonlinear problem can be solved analytically, that is, an exact solution has been obtained for the reflected wave formed in a perfect gas when a plane compression front steepens into a shock (Glass, Heuckroth & Molder 1961; Morfey & Sparrow 1993).

2. Formulation of the problem

We shall consider the strongly nonlinear propagation of plane waves generated by the sinusoidal motion of an infinite plate (see figure 1). The gas is initially uniform and at rest. At the time $t^* = 0$ the plate begins executing the harmonic oscillation of angular frequency ω and stops moving at $t^* = T \equiv 2\pi/\omega$.

The following non-dimensional variables are introduced:

$$t = \omega t^*, \quad x = kx^*, \quad u = \frac{u^*}{c_0}, \quad \rho = \frac{\rho^*}{\rho_0}, \quad p = \frac{p^*}{\gamma p_0}, \tag{2.1}$$

where $k = \omega/c_0$ is a typical wavenumber ($c_0 = (\gamma p_0/\rho_0)^{1/2}$), x^* is the space coordinate measured from the initial position of the plate, u^* is the fluid velocity, ρ^* is the density of the gas, and p^* is the pressure. The subscript 0 stands for the value at the initial undisturbed state. Thanks to condition (1.1b), we may use, as the equations governing the wave phenomena, Euler equations for a perfect gas:

$$\frac{\partial \boldsymbol{q}}{\partial t} + \frac{\partial \boldsymbol{f}}{\partial x} = 0, \tag{2.2}$$

with

$$\boldsymbol{q} = \begin{pmatrix} \rho \\ \rho u \\ E_t \end{pmatrix}, \quad \boldsymbol{f} = \begin{pmatrix} \rho u \\ p + \rho u^2 \\ (E_t + p)u \end{pmatrix}, \quad E_t \equiv \tfrac{1}{2}\rho u^2 + \frac{p}{\gamma - 1}. \tag{2.3a–c}$$

Until a shock forms, no dissipative process exists and hence (2.3*a–c*), the conservation law of energy, can be reduced to be $s_t + us_x = 0$, where s is the entropy per unit mass of the gas. In this case, since the flow field remains homentropic and a Riemann invariant becomes a constant in the wave region, the wave motion is governed by the so-called simple-wave equation (Courant & Friedrichs 1948):

$$\frac{\partial u}{\partial t} - \beta u \frac{\partial u}{\partial y} = 0 \quad \left(y = t - x,\ \beta \equiv \frac{\gamma + 1}{2} \right). \tag{2.4}$$

The boundary condition on the plate is given by

$$u = \begin{cases} M \sin t, & 0 \leqslant t < 2\pi \\ 0, & t < 0,\ t \geqslant 2\pi \end{cases} \quad \text{at} \quad x = M(1 - \cos t). \tag{2.5}$$

The initial condition is

$$u = 0 \quad \text{for} \quad x \geqslant 0 \quad \text{at} \quad t = 0. \tag{2.6}$$

In §4, equation (2.4) will be solved exactly subject to conditions (2.5) and (2.6).

Once a shock forms, the above simple-wave assumption becomes invalid by virtue of the presence of reflected waves behind the shock and the entropy production at the shock front (see Courant & Friedrichs 1948). We should therefore employ the full system (2.2) with (2.3) after the shock formation. This system omits effects of energy dissipation due to viscosity and thermal conduction, even though kinetic energy is in reality dissipated at the shock front. As is generally known, a shock solution can, however, be represented as a discontinuity, across which the conventional shock conditions must be satisfied. As the result, the thermoviscous effect is automatically included in this system. In order to describe such a situation mathematically, we need to introduce the concept of a weak solution to the system of equations (for example, see Jeffrey 1976 and LeVeque 1990). We shall numerically solve the system (2.2) with (2.3) so as to match the numerical solution with the exact solution obtained in §4, using a method based on the high-resolution upwind scheme as mentioned in the preceding section. The numerical procedure will in general choose a genuine solution from among many weak solutions, which exist mathematically.

3. Weakly nonlinear theory

Let us here recapitulate the well-known results for the weakly nonlinear case with $M \ll 1$ and $Re \gg 1$. The solution valid up to the distance of shock formation can be written in parametric form as (cf. Soluyan & Khokhlov 1961)

$$v = \sin \hat{y}, \quad \hat{y} = y + \sigma \sin \hat{y}, \quad 0 \leqslant \hat{y} \leqslant 2\pi, \tag{3.1}$$

where

$$v = u/M, \quad y = t - x, \quad \sigma = \beta M x. \tag{3.2}$$

This shows that the radiated sound wave has a sinusoidal profile at $\sigma = 0$, and the wave form distorts gradually as the wave advances, due to the weak nonlinearity.

The shock formation distance x_s and the shock formation time t_s are given as

$$x_{fs} = x_{rs} = x_s = \frac{1}{\beta M}, \quad \text{i.e.} \quad \sigma = 1, \tag{3.3}$$

and

$$t_{fs} = \frac{1}{\beta M}, \quad t_{rs} = \frac{1}{\beta M} + 2\pi \approx t_{fs}, \tag{3.4a,b}$$

where the subscript fs indicates the front (leading) shock and the subscript rs the rear (tail) shock. We remark that the front and the rear shocks emerge on $y = 0$ and $y = 2\pi$ respectively. The solution (3.1) becomes invalid beyond the point $\sigma = 1$, because it predicts that $u(y, t)$ becomes triple-valued for $\sigma > 1$. However, with the aid of the so-called equal-areas rule, we can easily analyse the propagation of a weakly nonlinear wave after the shock formation (see Landau & Lifshitz 1959; Whitham 1974).

We readily find the velocity amplitude (jump) of the two shocks (see Blackstock 1966)

$$\Delta v = \frac{2(\sigma - 1)^{1/2}}{\sigma}. \tag{3.5}$$

After some simple calculation, we can derive the total length of the wave

$$\Delta x = 4\left((\sigma - 1)^{1/2} + \arcsin\frac{1}{(\sigma)^{1/2}}\right). \tag{3.6}$$

As is well known, we have a symmetric N-wave as the asymptotic form in the limit as $\sigma \to \infty$.

Finally, some features of the weakly nonlinear waves may be listed as follows.

(i) For propagation over a few wavelengths, the wave substantially behaves in accordance with the linear law. In the far field, the nonlinear effects accumulate enough to distort the wave profile significantly and at last a shock emerges at $\sigma = 1$.

(ii) The wave profile of the particle velocity retains a symmetry between the compressive phase ($v > 0$) and the rarefactive phase ($v < 0$), through the entire process of wave propagation. The point of symmetry moves with constant speed. The area under the compressive phase (or over the rarefactive phase) remains constant through the entire process of wave propagation (see Appendix A).

(iii) The front shock is formed at the head of the wave and the rear shock at the end of the wave. The strength of each shock attains a maximum at $\sigma = 2$. At long distances ($\sigma \gg 1$), the velocity amplitude is attenuated in inverse proportion to $\sigma^{1/2}$ and the wave length increases in proportion to $\sigma^{1/2}$.

(iv) Streaming, due to wave propagation, is absent.

(v) In the weakly nonlinear theory, both the perturbation pressure and the perturbation density are equal to the velocity v in the normalized form.

4. Strongly nonlinear sound wave

If we limit ourselves to the wave propagation up to the shock formation time t_s, for the present problem of $M = O(1)$, we can succeed in obtaining the analytical exact solution to the simple-wave equation (2.4) under the boundary condition (2.5) and the initial condition (2.6) (cf. Blackstock 1962; Inoue & Yano 1993). In this case,

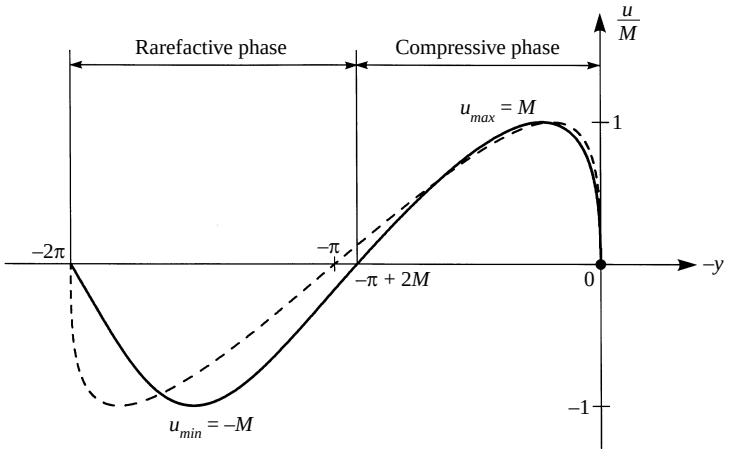

FIGURE 2. Velocity profiles just at the time when the front shock is formed. A strongly nonlinear wave for $M = 0.133$ is drawn with a solid line, and the weakly nonlinear wave with a broken line, at $t = t_s = 6.282$. The latter waveform exhibits a point symmetry about the point $(-y, u/M) = (-\pi, 0)$. The solid circle denotes the position where the front shock appears.

the waveform distortion takes place rather rapidly, contrary to the weakly nonlinear problem of small M in the preceding section.

The exact solution is expressible, through a parameter μ, as

$$u = M \sin \mu, \tag{4.1}$$

$$y - [\mu - M(1 - \cos \mu)] = \beta M(\mu - t) \sin \mu, \quad \text{with} \quad 0 \leqslant \mu \leqslant 2\pi, \quad \mu \leqslant t \leqslant t_s. \tag{4.2}$$

In what follows, we shall be concerned with the case $t_s \geqslant 2\pi$, i.e. $M \leqslant 1/[(\gamma + 1)\pi]$ (cf. (4.6)). Consequently, the source can radiate a localized sine-like wave before a shock is formed (see figure 2). The area of the compressive phase or the rarefactive phase remains constant during the wave propagation:

$$S_c \equiv \int_{\pi - 2M}^{0} u(y, t)\, \mathrm{d}y = 2M - \frac{\pi(2 - \beta)}{4} M^2. \tag{4.3}$$

Similarly, we have

$$S_r \equiv \left| \int_{2\pi}^{\pi - 2M} u(y, t)\, \mathrm{d}y \right| = 2M + \frac{\pi(2 - \beta)}{4} M^2, \tag{4.4}$$

and hence $S_c < S_r$. The lack of waveform symmetry is therefore due purely to specification of u on the displaced piston (plate) $x = X(t)$. This asymmetric feature is essentially different from the symmetric wave profile in the weakly nonlinear theory.

It is clear from inspection of (4.2) that the leading shock is formed at the wave front, so that we may deduce the same result that we have already obtained in the weakly nonlinear theory, namely (3.3) and (3.4*a*).

After the first shock is formed, the simple-wave theory becomes invalid. However, for moderate acoustic Mach number M, the front shock is initially weak. It does not then significantly influence the following wave region before the rear shock forms, at least. The formation time and formation distance of the rear shock can therefore be

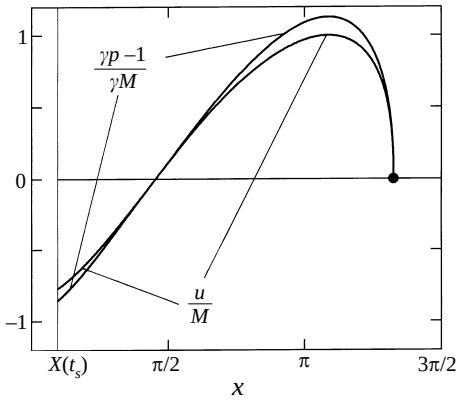

FIGURE 3. Comparison between the velocity and the excess pressure at the formation time of the front shock: $M = 0.2$, $\gamma = 1.4$.

given as follows (see Appendix B):

$$x_{rs} = \left[\frac{2\gamma}{\gamma+1}(v^2-1)^{1/2}\left\{v^2 - \frac{(\gamma+1)(2\gamma+1)}{2\gamma^2}\right\} - \frac{v}{\gamma}\right]\left(v^2 - \frac{\gamma+1}{2\gamma}\right)^{-1}, \tag{4.5}$$

$$t_{rs} = 2\pi + \arcsin\left(\frac{1}{v}\right) + \frac{2\gamma}{\gamma+1}(v^2-1)^{1/2}, \tag{4.6}$$

with

$$v \equiv \operatorname{cosec}\mu_{rs} = -\left[\frac{1}{2\gamma M} + \left(\left(\frac{1}{2\gamma M}\right)^2 + \frac{\gamma+1}{2\gamma}\right)^{1/2}\right]. \tag{4.7}$$

In fact, our numerical calculation shows that formulas (4.5)–(4.7) hold to a fairly good approximation, at least for $M \lesssim 1.2$ (when $M = 1.2$, estimated roughly, $t_{rs} = 2\pi$). In this approximation the rear shock formation occurs at a point (x_{rs}, t_{rs}) on a characteristic identified by $\mu = \mu_{rs}$ on which $u = M/v$ (< 0). The rear shock does not emerge at the tail of the wave, in contrast to the weakly nonlinear case. In the limit of weak nonlinearity as $M \to 0$, we recognize that the results (4.5) and (4.6) reduce to familiar formulas (3.3) and (3.4*b*) in §3. Moreover, it may be noted that solution (3.1) in the weakly nonlinear theory can be produced approximately by replacing t by x in (4.2) and representing (4.1) and (4.2) in terms of v and σ defined by (3.2) and then taking the limit $M \to 0$ in the resultant equation. We can also demonstrate that, up to the shock formation time, there exists no mean mass flow (streaming) (see Inoue & Yano 1993).

Profiles of velocity and perturbation pressure are depicted in figure 3, for the case of $M = 0.2$, $\gamma = 1.4$, and $t = t_{fs}$ $(\equiv 1/\beta M = 4.167)$. As is obvious from the figure, the two curves are distinct, unlike those of the weakly nonlinear wave (see §3). The shock formation distances given by (3.3) and (4.5) are illustrated for varying M in figure 4(*a*). This shows that, at least for $M \lesssim 1.2$, the formation distance of the front shock is larger than that of the rear shock, with M fixed, whereas $x_{fs} = x_{rs}$ in the weakly nonlinear theory (see §3). The shock formation times given by (3.4*a*), (3.4*b*), and (4.6) are illustrated for varying M in figure 4(*b*). These show that, as M increases, the formation time of the rear shock becomes even shorter compared to that extrapolated from the weakly nonlinear theory.

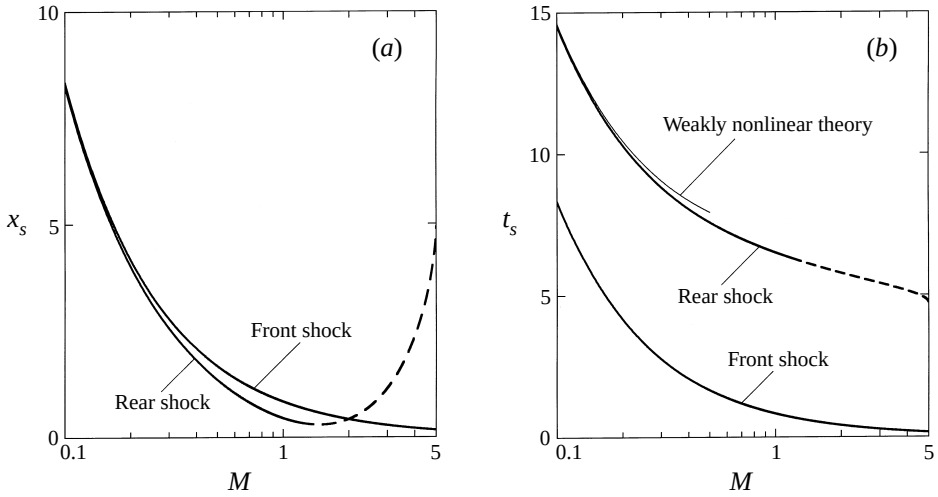

FIGURE 4. (*a*) Shock formation distances x_{fs} and x_{rs}. The broken line in x_{rs} denotes an unsupported extension obeying formula (4.5). (*b*) Shock formation times t_{fs} and t_{rs}. The result in the weakly nonlinear theory is indicated with a thin solid line.

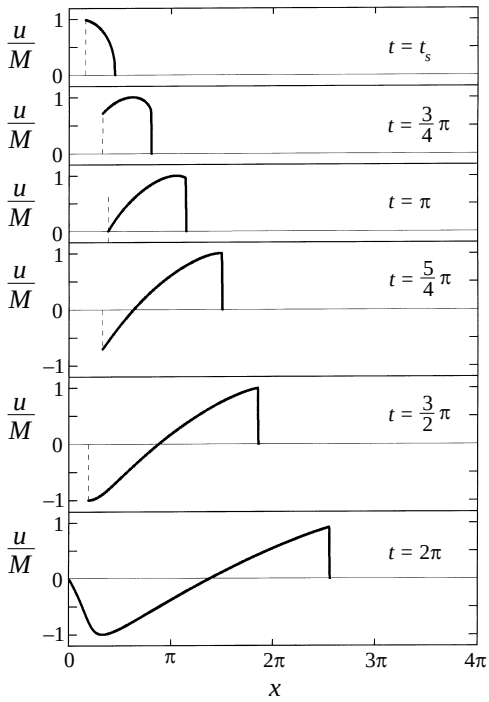

FIGURE 5. Time evolution of the velocity profile, according to the numerical calculation: the process up to the formation of an *N*-wave. $M = 0.6$, $\gamma = 1.4$; $(x_{fs}, t_{fs}) = (1.389, 1.389)$, $(x_{rs}, t_{rs}) = (1.035, 7.251)$. The broken line signifies the instantaneous location of the plate.

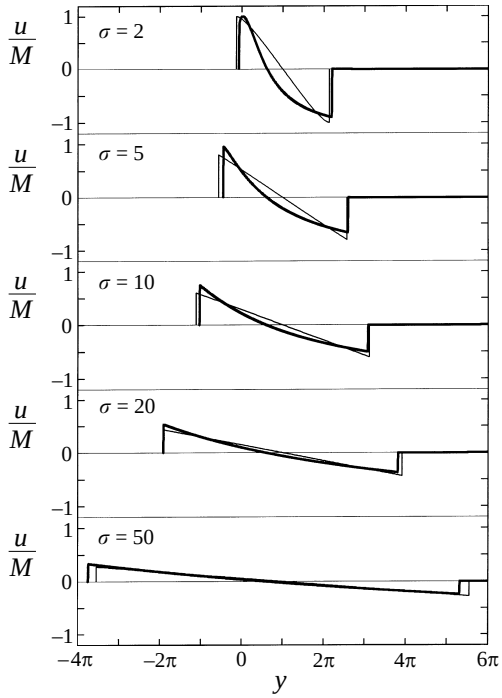

FIGURE 6. Change of the waveform with distance, $M = 0.6, \gamma = 1.4$. Each profile represents the temporal variation of the velocity observed at a fixed position. The result for the weakly nonlinear theory is indicated with a thin solid line.

5. Formation and evolution of a strongly nonlinear *N*-wave

For strong nonlinearity with $M = O(1)$, approximations such as the equal-areas rule are not valid, so that we adopt a numerical method, based on a high-resolution upwind difference scheme by Osher & Chakravarthy (1986). That is, we use the scheme together with Osher's flux-difference splitting (Osher & Solomon 1982). We need not give the algorithm to construct the numerical scheme here, since it is formulated at some length in Osher & Solomon (1982) and Osher & Chakravarthy (1986). The mathematical proofs of the validity of the scheme are also included in Osher & Chakravarthy (1986). The numerical calculation was performed on the supercomputer HITAC S–3800 at Hokkaido University. In what follows, we shall present the numerical results for the strongly nonlinear wave propagation under consideration, contrasting them with the results for the weakly nonlinear theory reviewed in §3.

5.1. *Strongly nonlinear N-wave: evolution of the wave including the two shocks and entropy production*

The velocity profiles at discrete times are shown in figure 5, for the case of $M = 0.6$ and $\gamma = 1.4$. Owing to the strong nonlinearity, the wave radiated from the plate develops into an N-like wave in the near field. At first sight, this might look like a wave profile evolving as the well-known N-wave in the weakly nonlinear theory. In order to make clearer contrast with the weakly nonlinear case, we examine changes of the wave profile with time at fixed points (see figure 6). As may be seen from figure 6, the form of the expansion wave between the two shocks is concave, while

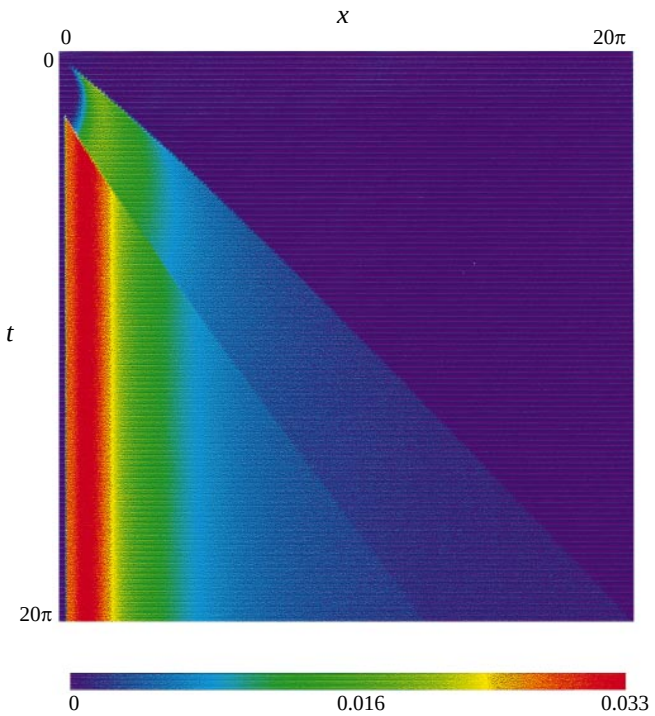

FIGURE 7. Entropy production that accompanies the formation and evolution of an N-wave: $M = 0.6$, $\gamma = 1.4$. The colour bar indicates values of the entropy increments.

the counterpart in the weakly nonlinear wave is almost a straight line. At the early evolutionary stage, the area of the rarefactive phase is large compared with the area of the compressive phase, whereas the situation reverses later. As mentioned before, in the weakly nonlinear theory the areas of these phases are equal and remain constant during the wave motion. At a great distance, the initially strongly nonlinear wave reduces to an ordinary N-wave with weak nonlinearity, but the resulting N-wave has no symmetry with respect to the point where $u = 0$, in marked contrast to the weakly nonlinear case.

In figure 7, encoded in colours, we present the space–time distribution of the entropy which is generated at the front and rear shocks. Since we take a perfect gas, the normalized entropy increment can be expressed as

$$s \equiv \frac{s^* - s_0}{c_v} = \ln \frac{\gamma p}{\rho^\gamma}, \tag{5.1}$$

where s_0 is the entropy per unit mass of the gas at the initial uniform state. We may here recall that the increase of entropy across a shock is given as

$$s = \ln \frac{(1+z)\left(1+[(\gamma-1)/2\gamma]\,z\right)^\gamma}{\left(1+[(\gamma+1)/2\gamma]\,z\right)^\gamma}, \quad z \equiv \frac{p_2 - p_1}{p_1} > 0. \tag{5.2}$$

Here p_1 and p_2 are the pressures immediately in front of and behind the shock front, and so we may regard z as the strength of the shock (for example, see Whitham 1974). The entropy produced by the shock increases monotonically with the strength z. As is evident from figure 7, the entropy is produced by each shock discontinuity, mainly by

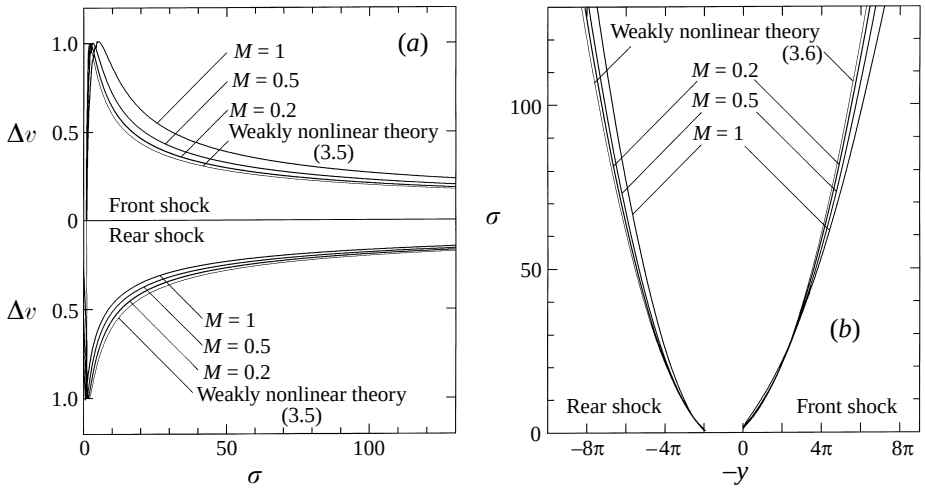

FIGURE 8. (*a*) Dependence of shock strength Δv on the distance σ. (*b*) Paths of the front shock and the rear shock in the (y, σ)-plane. The asymptotic forms are given by $y = \pi \pm 2\sigma^{1/2}$.

strong shocks at the early stage. As is generally known, the entropy is carried along by the gas flow, which is termed the entropy wave for convenience. Since the gas returns to an almost quiescent state after the second shock has passed, the gas having high entropy remains near the source (cf. §5.2). Finally we may remark that for weak shocks expression (5.2) can be expanded in powers of z as $s = [(\gamma^2-1)/12\gamma^2]\, z^3 + O(z^4)$ ($z \ll 1$), so motivating the usual neglect of entropy changes in the weakly nonlinear theory.

Figure 8(*a*) shows the change of the strength of the front and rear shocks with propagation distance $\sigma \equiv \beta M x$. We here define the strength of the shock as $\Delta v \equiv \Delta u/M = (u_2 - u_1)/M$, where u_1 and u_2 are the fluid velocities immediately in front of and behind the shock respectively (cf. (3.2)). The formula (3.5) based on the weakly nonlinear theory is designated by a thin solid line in figure 8(*a*). We see that for the front shock the aforementioned shock strength is enhanced as the acoustic Mach number M increases, whereas the result for the rear shock is the opposite. Clearly, even a wave which is initially strongly nonlinear eventually enters a weakly nonlinear regime, i.e. in the far field. In the weakly nonlinear theory, for the initial velocity distribution of a single hump, the asymptotic formula for $\Delta v(\sigma)$ is given by

$$\Delta v \sim (2A/\sigma)^{1/2} \quad \text{as} \quad \sigma \to \infty, \tag{5.3}$$

where A is the normalized area of the initial hump (phase) (see Whitham 1974). It seems that the asymptotic wave strength is somewhat affected by the asymmetric wave profile at the initial stage.

In figure 8(*b*) we depict the paths of the front and rear shocks in the (y, σ)-plane, where $y = t - x$ and $\sigma = \beta M x$. The thin solid lines denote the paths according to the weakly nonlinear theory given by (3.6). At the 'same time' the front shock with strong nonlinearity is located ahead of that in the weakly nonlinear limit, whereas the rear shocks are arranged in the reverse order in the y-direction. It may also be noted that the shock velocity is given by $u_s = (1 + \beta M \mathrm{d}y_s/\mathrm{d}\sigma)^{-1}$.

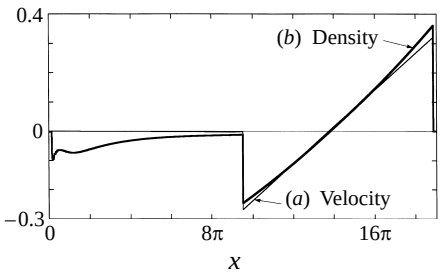

FIGURE 9. The profiles of an N-wave at $t = 14\pi$: $M = 1$, $\gamma = 1.4$. (a) The fluid velocity u. (b) The excess density $\rho - 1$. Clearly, a non-uniform region having low density exists behind the rear shock.

5.2. *The state behind the rear shock*

In the weakly nonlinear N-wave, after the rear shock passes the gas returns to its original uniform rest state. The profiles of the velocity and the density of a strongly nonlinear N-wave are shown in figure 9. The velocity u nearly vanishes behind the rear shock. On the other hand the perturbation density $(\rho - 1)$ has a non-zero distribution there, in marked contrast to the weakly nonlinear case. This fact is closely connected with the entropy production mentioned in the preceding subsection. At a rough estimate, we have the relation between the density and the entropy after a sufficiently long time,

$$\rho(x) = \exp\left[-s(x)/\gamma\right]. \tag{5.4}$$

This shows that the gas is rarefied in this region, that is $\rho(x) - 1 \leqslant 0$. The reduced mass is just counterbalanced by the positive excess mass accompanying the N wave (see the following subsection).

5.3. *Mass, momentum and energy of the N-wave and the region behind it*

The total mass and energy remain constant after the source motion has ceased, as can be estimated physically. On the other hand, integrating (2.3b), we have the corresponding total momentum

$$\int_0^\infty \rho u \,\mathrm{d}x = \int_0^\infty \rho u \,\mathrm{d}x\bigg|_{t=2\pi} + \int_{2\pi}^t \left[p(0,t) - \frac{1}{\gamma}\right] \mathrm{d}t, \tag{5.5}$$

where $p(0,t)$ denotes the pressure on the plate located at $x = 0$, for $t \geqslant 2\pi$.

Figure 10(a) shows the numerical result for the change of the total excess mass of the gas carried by the N-wave and that in the region behind the rear shock, as functions of time:

$$m_N(t) = \int_{\bar{x}_{rs}}^{\bar{x}_{fs}} (\rho - 1)\,\mathrm{d}x, \quad m_R(t) = \int_0^{\bar{x}_{rs}} (\rho - 1)\,\mathrm{d}x. \tag{5.6a, b}$$

Here, $\bar{x}_{fs}$ and $\bar{x}_{rs}$ denote the locations of the front shock and the rear shock respectively. The numerical result satisfies well the exact relation $m_N(t) + m_R(t) = 0$. This means that the N-wave has asymmetric density profiles even in the weakly nonlinear regime and asymmetric profiles for the other quantities, in marked contrast to the symmetric wave profiles in the weakly nonlinear theory.

We depict the total excess energy of the N-wave and that of the region behind the

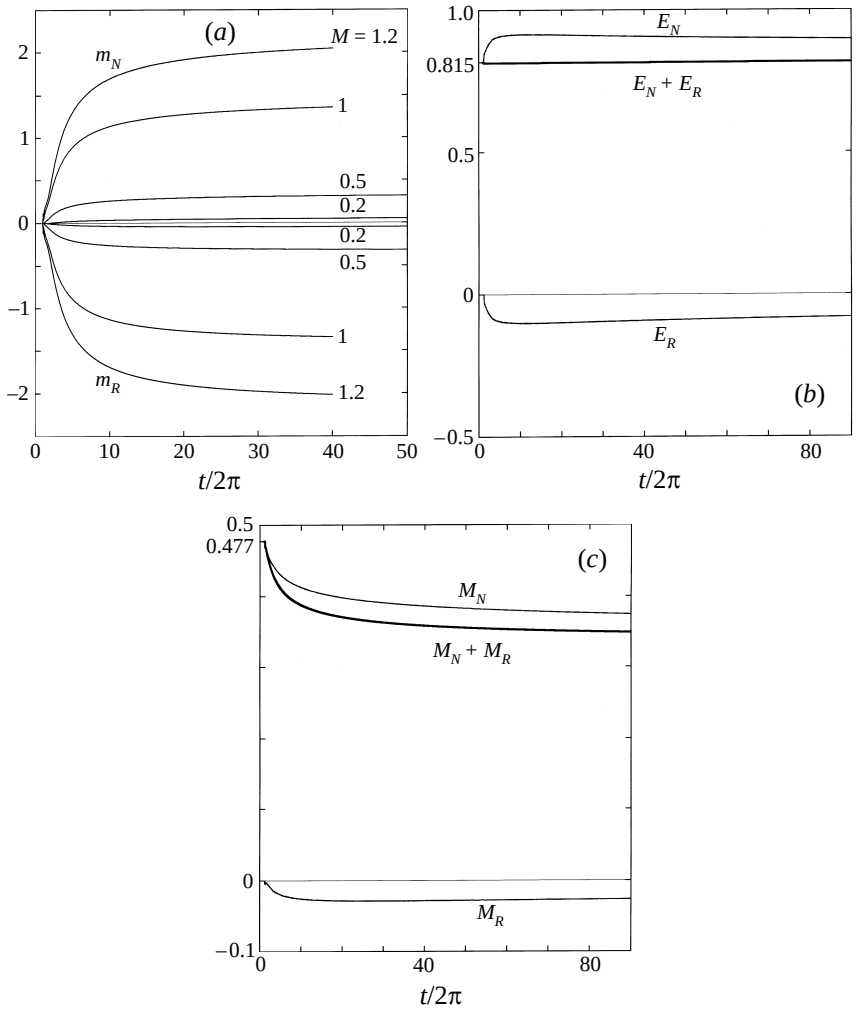

FIGURE 10. (*a*) Curves of the excess mass of the N-wave, m_N, defined by (5.6*a*) and of the remainder, m_R, defined by (5.6*b*), versus the time $t/2\pi$. $m_N + m_R = 0$. (*b*) Curves of the excess energy of the N-wave, E_N, defined by (5.7*a*) and of the remainder, E_R, defined by (5.7*b*), versus the time $t/2\pi$: $M = 0.5$, $\gamma = 1.4$. $E_N + E_R = 0.815$. (*c*) Curves of the momentum of the N-wave, M_N, defined by (5.11*a*) and of the remainder, M_R, defined by (5.11*b*), versus the time $t/2\pi$: $M = 0.5$, $\gamma = 1.4$. The total momentum of the entire field $M_N + M_R$ decreases as time proceeds.

N-wave in figure 10(*b*):

$$E_N(t) = \int_{\bar{x}_{rs}}^{\bar{x}_{fs}} \left(E_t - \frac{1}{\gamma(\gamma-1)} \right) \mathrm{d}x, \quad E_R(t) = \int_0^{\bar{x}_{rs}} \left(E_t - \frac{1}{\gamma(\gamma-1)} \right) \mathrm{d}x. \qquad (5.7a,b)$$

As the figure shows, $E_N(t) > 0$, $E_R(t) \leqslant 0$, and $E_N(t) + E_R(t) = 0.815$ for $t \geqslant t_{rs}$, when $M = 0.5$ and $\gamma = 1.4$. Now, it follows from the conservation law of energy that $E_N(t) + E_R(t) = \Delta E = \text{const}$. If the acoustic Mach number M is not too large, we can evaluate the energy increment ΔE. Integrating (2.3*c*) from the position of the plate, $X(t)$ to ∞ with respect to x and then from 0 to 2π with respect to t,

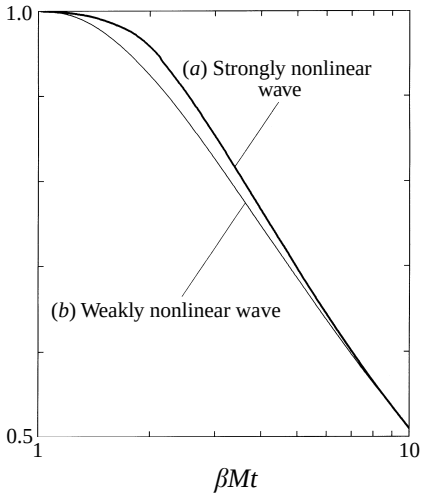

FIGURE 11. The loss of the kinetic energy of the N-wave due to the dissipation of energy at the shock fronts: (*a*) $(K.E.)_N/1.574\times10^{-2}$ (a strongly nonlinear wave with $M=0.1$ and $\gamma=1.4$), (*b*) $(K.E.)_N/(\pi M^2/2)$ (the weakly nonlinear wave).

we obtain

$$\Delta E=\int_0^{\infty}\left(E_t-\frac{1}{\gamma(\gamma-1)}\right)\mathrm{d}x\bigg|_{t=2\pi}=\int_0^{2\pi}p(X(t),t)\,u(X(t),t)\,\mathrm{d}t, \tag{5.8}$$

where we have used the Leibniz formula for the derivative of an integral. By making use of (4.1) and (4.2), we can calculate ΔE as follows:

$$\begin{aligned}\Delta E=&\ \frac{\pi M^2\,\Gamma(2)}{\Gamma\left(\dfrac{1}{1-\gamma}\right)\Gamma\left(\dfrac{\gamma+1}{2(1-\gamma)}\right)}\\&\times\sum_{m=0}^{\infty}\frac{\Gamma\left(m-\dfrac{1}{\gamma-1}\right)\Gamma\left(m-\dfrac{\gamma+1}{2(\gamma-1)}\right)}{\Gamma(m+2)m!}\left(\frac{(\gamma-1)M}{2}\right)^{2m}\\=&\ \pi M^2\,F\left(\frac{1}{1-\gamma},\frac{\gamma+1}{2(1-\gamma)},2\,;\,\frac{(\gamma-1)^2M^2}{4}\right),\end{aligned} \tag{5.9}$$

where Γ is the gamma function and $F(a,b,c;z)$ is known as the Gauss hypergeometric series. In the case $\gamma=1.4$ (for air), we obtain a finite series,

$$\Delta E=\pi\left(M^2+\frac{3}{20}M^4+\frac{3}{10^3}M^6+\frac{1}{2\times10^5}M^8\right). \tag{5.10}$$

This shows that $\Delta E=0.815$ for $M=0.5$, which agrees with the numerical result (see figure 10*b*).

Figure 10(*c*) shows that the total momentum of the whole fluid $M_N(t)+M_R(t)$ decreases with time, where

$$M_N(t)=\int_{\bar{x}_{rs}}^{\bar{x}_{fs}}\rho u\,\mathrm{d}x,\quad M_R(t)=\int_0^{\bar{x}_{rs}}\rho u\,\mathrm{d}x. \tag{5.11a,b}$$

In particular, the total momentum of the N-wave, $M_N(t)$, shows a steady decrease at the early stage, in marked contrast to the weakly nonlinear case in which it always holds that

$$M_N(t) = \int_{\bar{x}_{rs}}^{\bar{x}_{fs}} u \, \mathrm{d}x = 0. \tag{5.12}$$

As with the energy increment, we can evaluate exactly the momentum increment of the gas gained during the motion of the source:

$$\begin{aligned} \int_0^\infty \rho u \, \mathrm{d}x \bigg|_{t=2\pi} &= \int_0^{2\pi} \left(p(X(t), t) - \frac{1}{\gamma} \right) \mathrm{d}t \\ &= \frac{2\pi}{\gamma} \left[F\left(\frac{\gamma}{1-\gamma}, \frac{\gamma+1}{2(1-\gamma)}, 1 \, ; \, \frac{(\gamma-1)^2 M^2}{4} \right) - 1 \right]. \end{aligned} \tag{5.13}$$

For $\gamma = 1.4$, formula (5.13) is reduced to

$$\int_0^\infty \rho u \, \mathrm{d}x \bigg|_{t=2\pi} = \pi \left(\frac{3}{5} M^2 + \frac{3}{10^2} M^4 + \frac{1}{5 \times 10^3} M^6 \right), \tag{5.14}$$

which takes the value 0.477 for $M = 0.5$, in close agreement with the numerical result.

In figure 11 we depict the change of kinetic energy with time, for a strongly nonlinear N-wave with $M = 0.1$ and $\gamma = 1.4$ and the weakly nonlinear N-wave (see Appendix C). The curve represents the kinetic energy at the time $\tau = \beta M t$ divided by the kinetic energy at the initial time, say, $t = 2\pi$. In due course, the curve of the strongly nonlinear wave approaches asymptotically that of the weakly nonlinear wave, as the former wave enters the weakly nonlinear regime.

6. Conclusion

In this final section, we shall briefly summarize the results of the investigation which we have made on the strongly nonlinear N-wave in §§4 and 5. Thereby we shall see that the present strongly nonlinear N-wave has intriguing distinctive features, as contrasted with the well-known weakly nonlinear N-wave, that is, the N-wave in the conventional sense.

(i) Owing to the rapid waveform distortion due to the strong nonlinearity, shock waves appear in the near field. The first (front) shock is formed at $\sigma \equiv \beta M x = 1$, like in the weakly nonlinear case, whereas the second (rear) shock is formed at a shorter distance than the first shock, for $M \lesssim 1.2$. The second shock emerges after a timelag shorter than 2π after the first shock forms (cf. (i) in §3).

(ii) The wave profile does not have any symmetry between the compressive phase and the rarefactive phase through the entire process of wave propagation. Before the shock formation time, the velocity profile does not show a symmetry between the compressive phase and the rarefactive phase, as is evident from (4.3) and (4.4) (for $M < 1/[(\gamma+1)\pi]$). The wave profile continues to be asymmetric after the shock formation time. For instance, at the early stage of an N-wave, the expansion wave is very strong just behind the front shock and its strength decreases rapidly toward the rear shock. At large distances, the wave is reduced to an ordinary but asymmetric N-wave (cf. (ii) in §3).

(iii) The front shock is formed at the head of the wave but unlike the weakly nonlinear N-wave the rear shock is not formed at the tail of the wave. For the same σ, the 'normalized' strength of the strong shock, $\Delta v \equiv \Delta u / M$, is larger than that of

the weak front shock, whereas the situation is reversed for the rear shock (see figure 8*a*). At large distances, however, each strength approaches the strength of the weakly nonlinear limit. At the 'same' time $\tau = \beta M t$, both the strong front and rear shocks are located ahead of the front and rear shocks in the weakly nonlinear limit (cf. (iii) in §3).

(iv) Streaming caused by the wave propagation is weak compared with the streaming occurring in the strongly nonlinear sawtooth wave. As mentioned in §5 the fluid, as a whole, possesses some momentum and hence streaming in the region behind the rear shock after the strong N-wave has passed. However, it can approximately be neglected on a local scale (cf. (iv) in §3; see also Appendix D).

(v) The increment of entropy caused by strong shocks remains near the source, because the fluid would be almost at rest there after the N-wave has passed. This means that the density has a non-uniform distribution. Indeed, the numerical calculation supports this estimation well.

(vi) Some excess mass is carried along by the N-wave, as figure 10(*a*) shows. In the weakly nonlinear regime it can be deduced directly from the asymmetry of the waveform of the velocity.

Appendix A. Area-preserving propagation

On account of the symmetry of the wave profiles, it is sufficient to prove that the area under the compressive phase remains constant during the wave motion. Up to the shock formation, we can easily show it as follows:

$$S_c \equiv \int_0^{\pi} v \, \mathrm{d}y = \int_0^{\pi} \sin \hat{y}(1 - \sigma \cos \hat{y}) \, \mathrm{d}\hat{y} = 2. \tag{A 1}$$

We see that the result (A1) is also valid after the shock formation, thanks to the equal-areas rule. It may be noted that, strictly speaking, this property does not pertain to the N-wave solution of the Burgers equation (the detailed discussion is found in Whitham 1974).

Appendix B. Formation time and distance of the rear shock

The shock formation time must satisfy $(\partial u/\partial x)_t = -\infty$. We differentiate (4.2) with respect to x, with t being fixed, and then see that the condition yields

$$t = \mu + \frac{1}{\beta \cos \mu} \left[\frac{1}{M} + (\beta - 1) \sin \mu \right]. \tag{B 1}$$

Moreover, to seek the shock formation time, we should impose the additional condition that the right-hand side of (B1) takes a minimum:

$$\tfrac{1}{2}(\gamma + 1) \sin^2 \mu_{rs} - (1/M) \sin \mu_{rs} - \gamma = 0. \tag{B 2}$$

From (B2) we directly have (4.7). On the other hand, by making use of (B2), we can rewrite (B1) as

$$t_{rs} = \mu_{rs} - \frac{2\gamma}{\gamma + 1} \cot \mu_{rs} = \mu_{rs} + \frac{2\gamma}{\gamma + 1} [(\operatorname{cosec} \mu_{rs} + 1)(\operatorname{cosec} \mu_{rs} - 1)]^{1/2}, \tag{B 3}$$

and using (4.7) we can readily find the shock formation time given by formula (4.6).

In order to determine the shock formation distance, we may simply put $t = t_{rs}$ and

$\mu = \mu_{rs}$ in (4.2):

$$\begin{aligned} x_{rs} &= M(1-\cos\mu_{rs}) + (t_{rs}-\mu_{rs})(1+\beta M\sin\mu_{rs}) \\ &= M\left[1+\frac{(v^2-1)^{1/2}}{v}+\frac{2\gamma}{\gamma+1}(v^2-1)^{1/2}\left(\frac{1}{M}+\frac{\gamma+1}{2}\frac{1}{v}\right)\right]. \end{aligned} \tag{B 4}$$

An easy calculation shows that

$$M = -\frac{v}{\gamma}\left(v^2-\frac{\gamma+1}{2\gamma}\right)^{-1}. \tag{B 5}$$

Thus, we can bring (B4) into the expression (4.5) in terms of a parameter v.

Appendix C. Total kinetic energy of a weakly nonlinear *N*-wave

We may confine ourselves to examining the change of the total kinetic energy of the wave concerned after the shock formation. We can easily evaluate it with the aid of (3.1) and the equal-areas rule as follows:

$$\begin{aligned} (K.E.)_N &\equiv \int_{\bar{x}_{rs}}^{\bar{x}_{fs}} \tfrac{1}{2}u^2\,\mathrm{d}x = \tfrac{1}{2}M^2\int_{\bar{x}_{rs}}^{\bar{x}_{fs}} v^2\,\mathrm{d}x = \tfrac{1}{2}M^2\int_{\hat{y}_{fs}}^{\hat{y}_{rs}} \sin^2\hat{y}(1-\sigma\cos\hat{y})\,\mathrm{d}\hat{y} \\ &= \begin{cases} \tfrac{1}{2}M^2\left[\pi-\arcsin\dfrac{2(\sigma-1)^{1/2}}{\sigma}+\dfrac{10}{3}\dfrac{(\sigma-1)^{1/2}(\sigma-\frac{2}{5})}{\sigma^2}\right], & 1\leqslant\sigma\leqslant 2 \\ \tfrac{1}{2}M^2\left[\arcsin\dfrac{2(\sigma-1)^{1/2}}{\sigma}+\dfrac{10}{3}\dfrac{(\sigma-1)^{1/2}(\sigma-\frac{2}{5})}{\sigma^2}\right], & 2<\sigma, \end{cases} \end{aligned} \tag{C 1}$$

where $\hat{y}_{fs}$ and $\hat{y}_{rs}$ denote the y-coordinates of the front shock and the rear shock such that $\sin\hat{y}_{fs} = 2(\sigma-1)^{1/2}/\sigma$ and $\sin\hat{y}_{rs} = -2(\sigma-1)^{1/2}/\sigma$ (see (3.1) and (3.5)). In the limit as $\sigma\to\infty$, we have the asymptotic formula

$$(K.E.)_N = \tfrac{8}{3}M^2\sigma^{-1/2}. \tag{C 2}$$

Appendix D. Streaming in the one-dimensional problem

We can express the streaming, i.e. a time-averaged mass flux density $\langle\rho u\rangle$ as follows (see Inoue & Yano 1993):

$$\langle\rho u\rangle \equiv \frac{1}{2\pi}\int_t^{t+2\pi}\rho(x,t)u(x,t)\,\mathrm{d}t = -\frac{1}{2\pi}\int_0^x[\rho(x,t+2\pi)-\rho(x,t)]\,\mathrm{d}x, \tag{D 1}$$

where we have used the fact that $\langle\rho u\rangle_{x=0}$ for the present piston problem. This shows that the streaming has an immediate connection with the periodicity of the wave phenomenon concerned.

REFERENCES

Blackstock, D. T. 1962 Propagation of plane sound waves of finite amplitude in nondissipative fluids. *J. Acoust. Soc. Am.* **34**, 9–30.

Blackstock, D. T. 1966 Connection between the Fay and Fubini solutions for plane sound waves of finite amplitude. *J. Acoust. Soc. Am.* **39**, 1019–1026.

Courant, R. & Friedrichs, K. O. 1948 *Supersonic Flow and Shock Waves.* Wiley Interscience.

Crighton, D. G. & Scott, J. F. 1979 Asymptotic solutions of model equations in nonlinear acoustics. *Phil. Trans. R. Soc. Lond.* A **292**, 101–134.

DuMond, J. W. M., Cohen, E. R., Panofsky, W. K. H. & Deeds, E. 1946 A determination of the wave forms and laws of propagation and dissipation of ballistic shock waves. *J. Acoust. Soc. Am.* **18**, 97–118.

Earnshaw, S. 1860 On the mathematical theory of sound. *Phil. Trans. R. Soc. Lond.* **150**, 133–148.

Friedrichs, K. O. 1948 Formation and decay of shock waves. *Commun. Pure. Appl. Maths* **1**, 211–245.

Glass, I. I., Heuckroth, L. E. & Molder, S. 1961 One-dimensional overtaking of a shock wave by a rarefaction wave. *Am. Rocket Soc. J.* **31**, 1453–1454.

Hayes, W. D. 1971 Sonic boom. *Ann. Rev. Fluid Mech.* **3**, 269–290.

Hopf, E. 1950 The partial differential equation $u_t + uu_x = \mu u_{xx}$. *Commun. Pure. Appl. Maths* **3**, 201–230.

Inoue, Y. & Yano, T. 1990 Propagation of acoustic shock waves of large amplitude. In *Frontiers of Nonlinear Acoustics* (ed. M. F. Hamilton & D. T. Blackstock), pp. 141–146. Elsevier.

Inoue, Y. & Yano, T. 1993 Propagation of strongly nonlinear plane waves. *J. Acoust. Soc. Am.* **94**, 1632–1642.

Jeffrey, A. 1976 *Quasilinear Hyperbolic Equations and Waves.* Research Note in Mathematics 5. Pitman.

Landau, L. D. 1945 On shock waves at large distances from the place of their origin. *J. Phys. USSR* **9**, 496–500.

Landau, L. D. & Lifshitz, E. M. 1959 *Fluid Mechanics.* Pergamon.

LeVeque, R. J. 1990 *Numerical Methods for Conservation Laws.* Birkhauser.

Lighthill, M. J. 1956 Viscosity effects in sound waves of finite amplitude. In *Surveys in Mechanics* (ed. G. K. Batchelor & R. Davis), pp. 250–351. Cambridge University Press.

Lighthill, M. J. 1971 Supersonic boom theory. In *Shock Tube Research* (ed. J. L. Stollery, A. G. Gaydon & P. R. Owen). Chapman & Hall.

Lighthill, M. J. 1978 *Waves in Fluids.* Cambridge University Press.

Mendousse, J. S. 1953 Nonlinear dissipative distortion of progressive sound waves at moderate amplitudes. *J. Acoust. Soc. Am.* **25**, 51–54.

Morfey, C. L. & Sparrow, V. W. 1993 Plane compression front steepening in nonlinear media forms both a shock and a reflected wave. *J. Acoust. Soc. Am.* **93**, 3085–3088.

Nakamura, A. & Takeuchi, R. 1969 Propagation of finite amplitude sound pulses in air through a circular pipe. *Acustica* **22**, 88–95.

Osher, S. & Chakravarthy, S. R. 1986 Very high order accurate TVD schemes. In *Oscillation Theory, Computation, and Methods of Compensated Compactness* (ed. C. Dafermos, J. Ericksen, D. Kinderlehrer & M. Slemrod), pp. 229–274. Springer.

Osher, S. & Solomon, F. 1982 Upwind schemes for hyperbolic systems of conservation laws. *Math. Comput.* **38**, 339–377.

Pierce, A. D. 1993 Nonlinear acoustics research topics stimulated by the sonic boom problem. In *Advances in Nonlinear Acoustics* (ed. H. Hobæk), pp. 7–20. World Scientific.

Rudenko. O. V. & Soluyan, S. I. 1977 *Theoretical Foundations of Nonlinear Acoustics.* Plenum.

Sachdev, P. L. 1987 *Nonlinear Diffusive Waves.* Cambridge University Press.

Sachdev, P. L., Tikekar, V. G. & Nair, K. R. C. 1986 Evolution and decay of spherical and cylindrical *N* waves. *J. Fluid Mech.* **172**, 347–371.

Soluyan, S. I. & Khokhlov, R. V. 1961 Propagation of acoustic waves of finite amplitude in a dissipative medium. *Vestn. Moskov. Univ. Fiz. Astron.* **3**, 52–61.

Whitham, G. B. 1950 The behaviour of supersonic flow past a body of revolution, far from the axis. *Proc. R. Soc. Lond.* A **201**, 89–109.

Whitham, G. B. 1974 *Linear and Nonlinear Waves.* Wiley Interscience.

Yano, T. & Inoue, Y. 1993 Strongly nonlinear waves radiated by a circular piston. In *Advances in Nonlinear Acoustics* (ed. H. Hobæk), pp. 583–588. World Scientific.

Yano, T. & Inoue, Y. 1994 Numerical study of strongly nonlinear acoustic waves, shock waves, and streaming caused by a harmonically pulsating sphere. *Phys. Fluids* **6**, 2831–2844.